A Theoretical Study on the Effect of Surface Roughness on Mass Transport and Transformation in Biofilms

Cristian Picioreanu,[1,2] Mark C. M. van Loosdrecht,[1] Joseph J. Heijnen[1]

[1]Department of Biochemical Engineering, Delft University of Technology, Julianalaan 67, 2628 BC Delft, The Netherlands; telephone: +31 15 2781551; fax: +31 15 2782355; e-mail: C.Picioreanu@stm.tudelft.nl
[2]Department of Chemical Engineering, University Politehnica of Bucharest, Splaiul Independentei 313, 77206 Bucharest, Romania

Received 16 June 1999; accepted 22 November 1999

Abstract: This modeling study evaluates the influence of biofilm geometrical characteristics on substrate mass transfer and conversion rates. A spatially two-dimensional model was used to compute laminar fluid flow, substrate mass transport, and conversion in irregularly shaped biofilms. The flow velocity above the biofilm surface was varied over 3 orders of magnitude. Numerical results show that increased biofilm roughness does not necessarily lead to an enhancement of either conversion rates or external mass transfer. The average mass transfer coefficient and Sherwood numbers were found to decrease almost linearly with biofilm area enlargement in the flow regime tested. The influence of flow, biofilm geometry and biofilm activity on external mass transfer could be quantified by Sh–Re correlations. The effect of biofilm surface roughness was incorporated in this correlation via area enlargement. Conversion rates could be best correlated to biofilm compactness. The more compact the biofilm, the higher the global conversion rate of substrate. Although an increase of bulk fluid velocity showed a large effect on mass transfer coefficients, the global substrate conversion rate per carrier area was less affected. If only diffusion occurs in pores and channels, then rough biofilms behave as if they were compact but having less biomass activity. In spite of the fact that the real biofilm area is increased due to roughness, the effective mass transfer area is actually decreased because only biofilm peaks receive substrate. This can be explained by the fact that in the absence of normal convection in the biofilm valleys, the substrate gradients are still largely perpendicular to the carrier. Even in the cases where convective transport dominates the external mass transfer process, roughness could lead to decreased conversion rates. The results of this study clearly indicate that only evaluation of overall conversion rates or mass fluxes can describe the correct biofilm conversion, whereas interpretation of local concentration or flow measurements as such might easily lead to erroneous conclusions. *Biotechnol Bioeng* **68**: 355–369, 2000.
Keywords: biofilm; mathematical modeling; mass transfer; convection

INTRODUCTION

The substrate utilization rate is the key parameter in the design of biofilm processes used for wastewater treatment or in biotechnology. Two aspects are important when modeling steady-state biofilm processes: (1) substrate conversion rates in the biofilm and (2) substrate transport rates at the biofilm/liquid interface (external mass transport) and inside the biofilm (internal mass transport). Current mathematical models are based on diffusion-reaction balances of substrates in one-dimensional biofilm systems (Wanner and Reichert, 1996). External resistance to mass transfer is taken into account by mass transfer coefficients. These are calculated as a function of hydrodynamic conditions in the reactor, assuming basic shapes of biofilm surface (i.e., flat, spherical, etc.). Experimental evidence accumulated in recent years has shown that in some biofilms, heterogeneity can lead to significant two- or three-dimensional components of substrate fluxes (de Beer et al., 1996). In order to predict accurately substrate utilization rates, this experimental work should be interpreted within the context of a multidimensional model. Very little theoretical research has been done in the area of multidimensional biofilm models, due to (1) a lack of reliable experimental data and (2) complexity and cost of multidimensional computations. The increasing availability of powerful parallel computers in the recent years motivated our derivation of new two- and three-dimensional biofilm models (Picioreanu et al., 1998, 1999). Together with adequate experimental data, this new generation of models should be able to address many questions raised by the latest measurements of biofilm structural heterogeneity.

The hydrodynamic regime, biofilm surface geometry, substrate loading rates, and diffusivities are certainly affecting the rate of external mass transport (Bishop et al., 1997). Most of these factors are already contained in the present one-dimensional biofilm models. However, because of its multidimensionality, the effect of an irregular biofilm surface on mass transport and conversion rates has not been tackled on a theoretical basis. Zhang et al. (1994) concluded after a series of experiments that "the rougher the biofilm surface, the less the external mass transfer resistance." However, with respect to the effect of biofilm heterogeneity on conversion rates, it is equally important to specify: (1) at what scale was roughness defined and whether this is the

Correspondence to: C. Picioreanu

only relevant measure describing biofilm surface irregularity and (2) what was the range of fluid velocities in which the measurements were done. As we will demonstrate later, with respect to flow patterns over the biofilms, the standard definition of roughness is not enough to characterize the surface shape. Two "hilly" surfaces having the same standard deviation from the mean line (seen as the coefficient of roughness: Murga et al., 1995; Picioreanu et al., 1998) can expose very different surface areas. Roughness describes in general the depth of biofilm valleys. The width of the valleys, seen as the distance between separate clusters is also important, fact recently recognized also by Stoodley et al. (1999).

A main disputed problem is the relevance of convection in biofilm channels and pores. Since Stoodley et al. (1994) and Lewandowski et al. (1995) made clear that inert micrometer-sized particles can be transported through biofilm channels, the above problem continues to puzzle many biofilm researchers. Conceptual questions occur because the presence of flow itself does not necessarily mean that convective transport of nutrients is significant. De Beer and Stoodley (1995) experimentally demonstrated that, as expected, convection in biofilm valleys is significant only at high bulk flow velocities. By using a very simplified three-dimensional model, Rittmann et al. (1999) showed that the average flux of nutrient per carrier area can be increased by the cluster-and-channel type of biofilm *only if* there is enough convection in the open channels (that we call "valleys"). However, being based on pure diffusion-reaction mass balances, their model does not consider fluid dynamics and thus, cannot explain how and when convection would arise in the valleys. The mathematical model we formulate in this study does include fluid flow equations and can account for convective substrate transport. Thus, our models can explain, on a quantitative basis, when the substrate flux to the biofilm is really increased by liquid circulation in biofilm valleys.

A final goal should be finding mathematical correlations between mass transport parameters and the measures of biofilm heterogeneity. External mass transfer parameters in biofilms (e.g., Sherwood number) were often correlated with the hydrodynamic regime existing in the bioreactor (e.g., through Reynolds and Schmidt numbers). Geometrical ratios between different characteristic lengths of the full-scale system also enter these correlations under certain circumstances. However, geometrical parameters for microscale heterogeneity are rarely included in engineering correlations. Well-known examples are relations for friction factor calculation in turbulent flow through pipes, usually expressed as a function of pipe wall roughness. To our knowledge, no such experimental or theoretical correlation has been made between Sh number and a measure of biofilm surface irregularity (e.g., roughness, thickness, or area enlargement).

The aim of this study is to predict theoretically the influence of biofilm structural characteristics (roughness, compactness, or area enlargement as defined in Picioreanu et al. (1998)) on substrate (growth-limiting nutrients) mass transfer and conversion into the biofilm. Starting from basic principles of momentum and mass conservation laws, the goal is to predict mass transfer coefficients and conversion rates for different biofilm surface geometries. The significance of convective transport in biofilm systems will be also investigated from a theoretical point of view.

MODEL DESCRIPTION

Choice of the Model System

The computational biofilm system, Ω, is contained in a rectangular domain. It consists of two compartments (see Fig. 1): the bulk liquid Ω_1 and the solid biofilm Ω_2, separated by an interface Γ. Liquid flow is driven by moving the top plate with a constant velocity, $u_{X,max}$. The system resembles Couette flow between two parallel plates, with the biofilm surface at the bottom plate. Inlet and outlet flow boundaries (left and right sides on Fig. 1) are periodic, in order to minimize the entrance effects on the calculated flow pattern. This is as if, from a hydrodynamic point of view, the rough biofilm surface would continue infinitely and we compute the flow field only in a narrow window of it.

A no-slip condition (zero flow velocity) was set at the biofilm–liquid interface. According to Lewandowski et al. (1995) and Stoodley et al. (1997), the "biofilm" is defined as all the biomass clusters and liquid channels situated between a virtual plane at the maximum biofilm thickness, $\delta_{f,max}$, and the substratum. Using this definition, we might erroneously conclude that a slip boundary condition (i.e., non-zero components of velocities due to flow in the channels) must be set at the "biofilm" surface, i.e., at $y = \delta_{f,max}$. Whereas a one-dimensional biofilm model including fluid flow could use the slip-boundary, in a two-dimensional model the liquid phase and the biofilm phase (containing gel and biomass) can be completely separated. In our definition, *only* the biomass clusters belong to the "biofilm," so that a zero-velocity condition can be set at the gel–water interface.

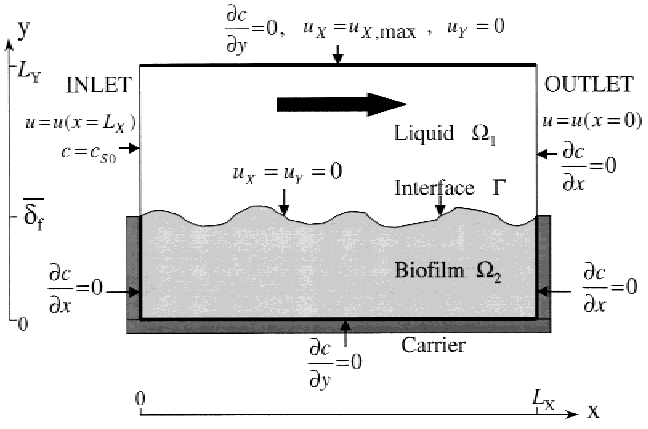

Figure 1. System description and boundary conditions.

However, there is a restriction also in this case: the no-slip boundary condition is valid only when the biofilm clusters are immobile. Many natural biofilms are flexible structures, and therefore oscillations induced by the flow can occur (Stoodley et al., 1998). This movement can create turbulence and can enhance the mass transfer of nutrients (Kugaprasatham et al., 1992). Although in some cases mobile biofilm filaments are probably more relevant, for simplicity, our present model considers only rigid and immobile structures.

For the mass transfer equation, a constant substrate concentration is fixed at the inlet boundary. The zero concentration gradient condition is specified at the outlet boundary. We assume that the thickness of the concentration boundary layer is smaller than the height of our computational domain. Consequently, a zero flux condition is applied also on the top boundary. The biofilm layer extends over the whole carrier surface, having for all simulated cases an average thickness of $\bar{\delta}_f = 145$ μm. Impermeable walls border the biofilm at left, right and bottom side (Fig. 1). The above conditions imply a "fully developed" flow field but an "entrance region" regime for mass transfer, which is the consequence of liquid flow in a closed system, while mass transport of substrate occurs in an open system. There are several good reasons for using such an idealized system.

First, the choice of this model system has its roots in a scale analysis of momentum and mass boundary layers. The relative thickness of the two boundary layers is determined by the cubic root of Schmidt number (Sc). Due to the high Sc numbers (e.g., 500) in liquid systems, the hydrodynamic boundary layer (HBL) is much thicker than the concentration boundary layer (CBL) (e.g., by a factor 8). When the entire concentration boundary layer is embedded within a small part of the momentum boundary layer, one may assume a linear velocity profile. This is in fact the Lévêque approximation employed in the similarity solution for the entrance region of a tube with specified wall concentration or temperature (Graetz problem; for example, see Deen, 1998). This linearization reflects the fact that the curvature in the parabolic velocity profile is not evident very near the walls. Couette flow between two parallel plates would produce exactly this linear x velocity profile, if only the biofilm surface was perfectly flat. What we calculate here is in fact a perturbation of this velocity profile due to a solid rough biofilm boundary. Experimental evidence supporting this assumption can be found in Stoodley et al. (1994), de Beer and Stoodley (1995), Lewandowski et al. (1995), Bishop et al. (1997), and Stoodley et al. (1997). All these studies measured liquid velocity and concentration profiles near to the wall of a flow cell with and without biofilm. They found velocity profiles approximately linear up to 500–1000 μm away from the biofilm surface, for average bulk liquid velocities between 0.001 and 0.1 m/s. The CBL was observed to be contained within this thickness. In the present modeling study we used top liquid velocities (at 255 μm above the average biofilm surface) varying over 3 orders of magnitude from 0.0001 to 0.13 m/s. Our calculations are therefore performed only in this quasi-linear region of the HBL. In reality, velocity continues to vary in the whole liquid layer above the biofilm. Because most of the experimental studies report only average or maximum velocity in the liquid, it is useful to show how the maximum velocity in the model system is correlated with the average velocity. We can take as example velocities those measured by Stoodley et al. (1994) in a closed planar flow cell with 1 cm liquid film. If our velocity profiles would be extrapolated through the whole liquid film, assuming parabolas with zero velocity gradient at 0.5 cm, then average flow velocities between 7×10^{-4} and 0.8 m/s would be obtained. Except for the very high velocities, these values are in the range of velocities existing in biofilm reactors (Kissel, 1986; Horn and Hempel, 1995; Bishop et al., 1997). It must be noted that in the high Re regime, the linear approximation of the velocity profile refers to the laminar sublayer. Due to the existence of turbulent eddies it is possible that the Couette flow approximation is not valid at turbulent flow.

Second, the system can be seen as an idealized rotating annular biofilm reactor, as described in Gjaltema et al. (1994). In old (5 days and over) or thick biofilms (>100 μm), sinusoidal dune-like ridges formed perpendicular to the flow direction. In these *Pseudomonas aeruginosa* biofilm, the ridges were about 100 μm apart. The long extension of the ridges in the direction perpendicular to the flow velocity vector allows for a reasonable two-dimensional description. The system can be also considered a model of the hydrodynamic (sub)laminar layer formed in the flow cell used by Stoodley et al. (1994) or de Beer and Stoodley (1995).

Finally, the third reason for selecting the Couette-like biofilm system is a faster convergence of the numerical solutions to the momentum and mass balances. It is known that iterative methods for partial differential equations converge faster to the steady-state solution when fixed-value ("essential" or "Dirichlet") boundary conditions are applied rather than in the case when the normal component of the gradient of property is specified ("natural" or "Neumann" conditions). Therefore, specifying a velocity at the top boundary ($y = L_Y$) is a computational advantage over imposing the zero gradient condition that would be necessary for a complete momentum boundary layer.

Model Equations

Our goal is to find the global rate of substrate conversion in the biofilm volume, under different flow conditions, for various biofilm surface shapes and various biofilm activities. Thus, the influence of biofilm roughness on the local and global mass transfer coefficients will also be computed. The global rate can be found by integrating the local consumption rates over the biofilm volume. The local substrate consumption rate, $r_S(x,y)$, depends on the local concentration of dissolved limiting substrate(s) through a kinetic expression (i.e., Monod kinetics). Consequently, if we assume only one limiting substrate (e.g., dissolved O_2), its distribu-

tion in space, $c_S(x,y)$, must be calculated from a mass balance equation, set-up in the whole domain Ω. At steady state, the convection–diffusion-reaction mass balance is:

$$\mathbf{u} \cdot \nabla c_S = D_S \nabla^2 c_S - r_S\,(c_S, c_X), \tag{1}$$

where D_S is the substrate diffusion coefficient, r_S is the rate of substrate consumption, c_S and c_X are the concentrations of substrate and biomass, respectively, ∇ is the divergence operator, and ∇^2 is the Laplacian operator with respect to the spatial coordinate **x.** In the biofilm domain, Ω_2, the convective transport term (left-hand side of Eq. (1)) equals zero because $\mathbf{u} = 0$, whereas in the liquid domain, Ω_1, the substrate consumption is zero because we assume no significant substrate uptake by suspended biomass ($c_X \approx 0$, thus r_S cf. Eq. (3) is zero).

Boundary conditions associated with Eq. (1) are

$$c_S(0,y) = c_{S0} \qquad \text{in inlet, at } y \in [\bar{\delta}_f, L_Y], \tag{2a}$$

$$\frac{\partial c_S}{\partial x}(L_X,y) = 0 \qquad \text{in outlet, at } y \in [\bar{\delta}_f, L_Y], \tag{2b}$$

$$\frac{\partial c_S}{\partial y}(x,y) = 0 \qquad \text{on the top and bottom boundaries, at } x \in [0,L_X],\ y = 0,\ y = L_Y, \tag{2c}$$

$$\frac{\partial c_S}{\partial x}(x,y) = 0 \qquad \text{on the impermeable side walls, at } x = 0,\ x = L_X,\ y \in [0,\bar{\delta}_f). \tag{2d}$$

No explicit internal boundary condition is set on the surface Γ, because we assume equal diffusion coefficients in liquid and in the biofilm phase. This ensures the continuity of mass fluxes over the biofilm-liquid interface. The rate of substrate (oxygen in our case) consumption in the biofilm is given by a Monod function:

$$r_S = \frac{\mu_m}{Y_{XS}} c_X \frac{c_S}{K_S + c_S} = k_{Sm} \frac{c_S}{K_S + c_S} \qquad (\text{in } \Omega_2). \tag{3}$$

In the model formulation, maximum biomass growth rate, μ_m, yield of biomass on oxygen, Y_{XS}, and the biofilm biomass density, c_X, were lumped into one constant parameter, k_{Sm}, the maximum oxygen consumption rate. This was possible because we assume a constant biomass density in the entire biofilm volume. Also, the model assumes biomass growth to be in frozen-state. In the following, k_{Sm} will be referred as a measure of the biofilm activity.

The steady-state field of velocity, $\mathbf{u} = (u_X, u_Y)$, used to support the convective transport of substrate is given by the incompressible Navier–Stokes equations in the laminar regime:

$$\mathbf{u} \cdot \nabla \mathbf{u} = -\frac{1}{\rho} \nabla p + \nu \nabla^2 \mathbf{u}, \tag{4}$$

$$\nabla \cdot \mathbf{u} = 0, \tag{5}$$

where $\mathbf{u}$ is the vector of liquid velocity, p is the pressure, ρ is the liquid density, and ν is the liquid kinematic viscosity. Two-dimensional Navier–Stokes equations are solved in the domain Ω_1 with boundary conditions:

$$u_X = u_Y = 0 \qquad \text{on biofilm–liquid interface } \Gamma, \tag{6a}$$

$$\left.\begin{aligned} u_X(0,y) &= u_X(L_X,y) \\ u_Y(0,y) &= u_Y(L_X,y) \end{aligned}\right\} \qquad \text{in inlet and outlet, at } y \in [\bar{\delta}_f, L_Y], \tag{6b,c}$$

$$\left.\begin{aligned} u_X(x,L_Y) &= u_{X,max} \\ u_Y(x,L_Y) &= 0 \end{aligned}\right\} \qquad \text{on the top boundary, at } x \in [0,L_X]. \tag{6d,e}$$

Model Parameters

Typical parameters in biofilm systems were used throughout this study, as listed in Table I. The length of the system, 1.6 mm, is large enough to have a biofilm patch representative for observation of roughness effects on substrate mass transfer. Biofilm average thickness is taken to be 145 μm, with variations between 50 and 250 μm. Biofilm ridges, 100–500 μm apart, were separated by valleys 100–200 μm deep, as observed in rotating annular bioreactors by many researchers (e.g., Gjaltema et al., 1994). The thicknesses of biofilms observed in mass transfer studies by de Beer et al.

Table I. Model parameters.

Model parameter	Symbol	Parameter value	Units
Computational grid dimensions	$N_X \times N_Y$	480 × 240 for Re = 0.032 to 0.255 480 × 120 for Re = 0.510 to 32.64	–
Physical system dimensions	$L_X \times L_Y$	1,600 × 800 for Re = 0.032 to 0.255 1,600 × 400 for Re = 0.510 to 32.64	μm
Average biofilm thickness	$\bar{\delta}_f$	145	μm
Bulk oxygen concentration	c_{S0}	10^{-3}	$kg_s\ m^{-3}$
Oxygen maximum consumption rate	k_{Sm}	1.136×10^{-3} for high-activity biofilm 2.272×10^{-4} for low-activity biofilm	$kg_s\ m^{-3}\ s^{-1}$
Oxygen saturation constant	K_S	10^{-4}	$kg_s\ m^{-3}$
Oxygen diffusion coefficient	D_S	2.3×10^{-9}	$m^2\ s^{-1}$
Liquid kinematic viscosity	ν	10^{-6}	$m^2\ s^{-1}$
Liquid density	ρ	1000	$kg\ m^{-3}$
Liquid velocity on top boundary	$u_{X,max}$	0.125×10^{-3}; 0.25×10^{-3}; 0.5×10^{-3}; 1×10^{-3}; 2×10^{-3}; 4×10^{-3}; 8×10^{-3}; 16×10^{-3}; 32×10^{-3}; 64×10^{-3}; 128×10^{-3}	$m\ s^{-1}$
Re number	Re	0.032; 0.064; 0.128; 0.255; 0.51; 1.02; 2.04; 4.08; 8.16; 16.32; 32.64	–

(1994, 1996), de Beer and Stoodley (1995), Lewandowski et al. (1995), and Stoodley et al. (1997) were also in this range. The height of the computational domain, 0.4 mm, contained all the concentration boundary layer, except for the case simulated at the lowest Re (Re defined by Eq. (9)). Because of this, at very low Re (between 0.032 and 0.255), the system height was extended to 800 μm. A wide range of fluid velocities within the laminar regime and comparable with those in biofilm reactors (Kissel, 1986) were applied. Kinetic parameters for substrate consumption in the biofilm were taken within the natural range of values for microorganisms in water treatment systems (Tijhuis et al., 1994). Dissolved oxygen with an inlet concentration of 1 mg/L was assumed the limiting substrate. Simulations at two values of k_{Sm} were performed: one corresponding to a highly active biofilm and the other one to a low activity biofilm. D_S was the diffusion coefficient for oxygen in water.

Thirteen different biofilm structures were numerically generated. A spline interpolation procedure between a certain number of points was used to generate the biofilm surface shape between a minimum and a maximum chosen height. The generated structures were constrained by two measures. First, the biofilm volume, V_b, was always the same, containing the same biomass density, uniformly distributed. Secondly, all structures had the same average biofilm thickness, $\bar{\delta}_f = 145$ μm. Compactness, area enlargement and roughness calculated for all model structures as shown in section "Measures of Biofilm Structure" are presented in Table II. A completely flat structure was taken as reference.

Model Solution

Both momentum and mass transfer equations were solved with nine-speed lattice Boltzmann (LB) methods (Ponce Dawson et al., 1993; Chen and Doolen, 1998). Our LB algorithms have been successfully tested in several convection–diffusion-reaction systems (Picioreanu, 1999). The main advantages of the LB method are the inherent algorithmic parallelism and programming simplicity. It is relatively easy to incorporate irregular boundaries and mesh generation is trivial at least for the uniform grid LB. An efficient parallelisation of LB algorithm was done by grid partitioning. All model simulations reported here were performed either on 8 or on 16 processors from the Cray T3E of the Center for High Performance Applied Computing in Technical University Delft.

Both momentum and mass transfer equations were discretised on a grid with 480 nodes in the flow direction (x). 120 nodes across the flow (y direction) were used for Re from 0.51 to 32.6, whereas 240 nodes were used between Re = 0.032 and 0.255. The lattice step size was $\Delta x = 3.36 \times 10^{-6}$ m, the same in both directions. The time step size was fixed to $\Delta t_f = 1.88 \times 10^{-6}$ s for flow calculations. For mass transport and reaction, the time step varied from $\Delta t_m = 8 \times 10^{-3}$ (at Re = 0.032) to 8×10^{-6} s (at Re = 32.6).

Table II. Structural parameters for the biofilms simulated.

Structure	Compactness ξ	Area enlargement α	Roughness σ
0 (flat)	1.000	1.000	0.000
1	0.910	1.025	0.043
2	0.857	1.042	0.070
3	0.777	1.104	0.090
4	0.712	1.092	0.127
5	0.609	1.276	0.155
6	0.506	1.382	0.240
7	0.425	1.645	0.195
8	0.414	1.779	0.165
9	0.399	1.480	0.324
10	0.301	2.084	0.254
11	0.300	1.969	0.296
12 (very rough)	0.211	2.543	0.340

Mass Transfer Coefficients

By definition, the local mass transfer coefficient results from the equality of normal components of mass fluxes at the biofilm–liquid interface, Γ:

$$\Phi_n = k_s(c_{S0} - c_{S,\Gamma}) = -D_S \left.\frac{\partial c_S}{\partial n}\right|_\Gamma, \tag{7}$$

where n is a coordinate normal to the biofilm surface (positive direction outward) and the subscript Γ denotes evaluation at the interface (Deen, 1998). Practical information on mass transfer coefficients is correlated most efficiently using Sherwood number (Sh), a dimensionless form of mass transfer coefficient:

$$\mathrm{Sh} = \frac{k_s L_h}{D_S} = \frac{-L_h \left.\frac{\partial c_S}{\partial n}\right|_\Gamma}{(c_{S0} - c_{S,\Gamma})}. \tag{8}$$

Sh values, as well as Reynolds numbers (Re), depend on the characteristic length chosen. Therefore, comparison of data measured in diverse systems should be done with great care when using dimensionless numbers. In this study the relevant length for hydrodynamics is the average height of the flow channel, $L_h = L_Y - \bar{\delta}_f = 255$ μm. This is the length used both in Sh and in Re numbers, so that

$$\mathrm{Re} = u_{X,\max} L_h/\nu. \tag{9}$$

When the total rate of mass transfer from surrounding liquid to the solid biofilm is calculated, the key quantity is the average Sherwood number, $\overline{\mathrm{Sh}}$. Averaging Eq. (8) over the biofilm surface S_Γ yields the expression for $\overline{\mathrm{Sh}}$:

$$\overline{\mathrm{Sh}} = \frac{1}{A_\Gamma} \int_{S_\Gamma} \mathrm{Sh}\, dS_\Gamma, \tag{10}$$

where A_Γ is the biofilm surface area. All $\overline{\mathrm{Sh}}$ numbers reported in this article were averaged over the biofilm surface between $x = 100$ μm and $x = 1{,}500$ μm. The first and last

100 μm were eliminated in order to diminish unwanted boundary effects.

The strict fractional definition for the concentration boundary layer thickness is at 99% of the bulk fluid concentration. Due to its thickness variation over the length, it is more convenient to calculate an averaged CBL thickness as $\bar{\delta}_b = D_S/\bar{k}_S$. The averaged mass transfer coefficient, $\bar{k}_s$, comes by substituting $\overline{Sh}$ in Eq. (8). $\bar{\delta}_b$ is used in this work only for a qualitative comparison of different flow regimes and biofilm geometries.

Global Substrate Consumption Rate

The *total substrate consumption rate* in the biofilm can be calculated by several methods. In practice, the total substrate consumption rate is found from a mass balance of substrate over the whole system, which equates the overall rate of substrate accumulation to the rates of entry and consumption. Assuming the system at steady-state, the conversion rate of substrate in the biofilm, Q_{react}, must be the difference between the rate at which the substrate enters the control volume, Q_{in}, and the rate of exit, Q_{out}. Substrate enters and exits the system only with the liquid flow. In our model system, the mass flow-rates can be calculated by integrating the convective fluxes over the inlet and outlet surfaces. By using the trapezoidal integration scheme, for a hypothetical biofilm depth L_Z, the inlet mass flow rate is:

$$Q_{in} = \int_{S_{in}} \Phi_{in,n} dS \approx \sum_{j=1}^{N_Y-1} 0.5[u_X(1,j)c_S(1,j) + u_X(1,j+1)c_S(1,j+1)]\Delta y L_Z. \quad (11)$$

A similar expression applies also for Q_{out}.

A second alternative is to compute the overall rate of substrate transfer across the biofilm–liquid interface Γ. Assuming all substrate that enters the biofilm must be converted and that reaction occurs only in the biofilm volume, the rate of substrate transfer, Q_{tr}, must equal the global reaction rate, Q_{react}. The rate of substrate transfer across the interface Γ can be obtained by integrating the substrate flux over the biofilm surface. Using the concentration values in the grid nodes located next to Γ interface, $c_{S,\Gamma+}(i,j)$ and $c_{S,\Gamma-}(i,j)$, and a centered approximation of the derivative, the substrate flow rate over the biofilm interface is:

$$Q_{tr} = \int_{S_\Gamma} \Phi_{n,\Gamma} dS_\Gamma = \int_{S_\Gamma} \left(-D_S \left.\frac{\partial c_S}{\partial n}\right|_\Gamma \right) dS_\Gamma \approx \sum_{(i,j)\in\Gamma} \left(-D_S \frac{c_{S,\Gamma+}(i,j) - c_{S,\Gamma-}(i,j)}{2\Delta n} \right) \Delta n L_Z. \quad (12)$$

The third option is to directly integrate the substrate conversion rate over the biofilm volume, V_b. By substituting in the reaction rate the substrate concentrations in the grid nodes, and summing up contributions of all grid volumes, the global substrate conversion rate is:

$$Q_{react} = \int_{V_b} r_S dV \approx \sum_{(i,j)\in V_b} r_S(c_S(i,j))\Delta x \Delta y L_Z. \quad (13)$$

We calculated the global substrate conversion rate by all three methods. The results differed in a range of ±2%. The differences can be attributed to integration and differentiation errors or to inaccuracy in the concentration and velocity fields obtained by the lattice Boltzmann method (see below). Because numerical integration is usually less erroneous than numerical differentiation, all results presented in this study calculated the global conversion rate using volume integration method.

Once the rate of substrate conversion is known, measures of biofilm effectiveness can be calculated. Because the global conversion rate is an extensive measure, $[M \cdot T^{-1}]$, and we compute in a two-dimensional space, a biofilm depth dimension must be defined together with the already known L_X and L_Y. More useful measures to compare mass transfer and transformation are the intensive ones, like the substrate *conversion rate per carrier area,* $\Phi_{S,C}$ (with flux units, i.e., g substrate · $m^{-2}_{carrier}$ · day^{-1}), given by:

$$\Phi_{S,C} = \frac{Q_{react}}{L_X L_Z}, \quad (14)$$

where the carrier area is $A_C = L_X L_Z$. The *global effectiveness factor* of the biofilm, η, can be calculated as in traditional chemical engineering (Fogler, 1992) as being the ratio between the actual conversion rate and the rate that would result if the entire volume would be exposed to the bulk concentration, c_{S0}:

$$\eta = \frac{Q_{react}}{\int_{V_b} r_S(c_{S0}) dV}. \quad (15)$$

Measures of Biofilm Structure

We will use here a few selected statistical quantities to characterize the internal and external structure of simulated biofilms, as given in Picioreanu et al. (1998). These will be needed to quantitatively compare the effect of different biofilm morphology on substrate mass transfer and transformation.

a. *Biofilm surface area enlargement,* α, is the ratio between the real biofilm surface area, A_Γ, and the carrier area, A_C. At a complete carrier coverage, the surface enlargement coefficient takes values greater than 1, meaning that a waved biofilm surface is larger than the bare surface. A patchy biofilm can have $\alpha < 1$.

b. *Biofilm surface roughness* is a measure that takes into account the depth of biofilm irregularities. It characterizes the variation from the mean elevation of a surface (Zhang et al., 1994). The coefficient of surface roughness is a dimensionless number $\sigma = \sigma_f/\bar{\delta}_f$, where σ_f is the absolute deviation of biofilm front points from the mean biofilm thickness

$\bar{\delta}_f$, as defined in Picioreanu et al. (1998). The smaller σ, the smoother the biofilm surface, while a high value of σ means a rough or patchy biofilm.

c. *Biofilm compactness,* ξ. Although area enlargement and roughness capture well the biofilm shape characteristics, we have found that the relationship between $\Phi_{S,C}$ and biofilm shape is better correlated by a measure called compactness. Compactness is defined in our system is an adaptation of the traditional *shape factor,* widely used in image analysis. Compactness, ξ, is the net volume (V_b) of a biofilm with maximum thickness $\delta_{f,max}$ relative to the volume of a hypothetical rectangular parallelepiped biofilm having the same liquid-solid area as the actual biofilm surface ($N_X\alpha$). It reads: $\xi = V_b/(\delta_{f,max}N_X\alpha)$. The measure takes its largest value 1 for a compact and completely flat biofilm. Any departures in the biofilm shape from the flat geometry (such as a border rather irregular than smooth) will decrease the measure. Compactness is a routinely measured shape property in image analysis.

RESULTS AND DISCUSSION

In correlating information on external mass transfer, either experimental or theoretical, we are concerned with the minimum set of dimensionless variables on which they depend. These variables can be identified by inspecting the governing equations, that is, Navier–Stokes, mass balance, and kinetic equations. It follows from these equations that the local Sh number has the functional dependence:

$$\mathrm{Sh} = \mathrm{Sh}\ (\mathbf{x}_\Gamma, \mathrm{Re}, \mathrm{Sc}, \phi^2, K, \text{geometric ratios}), \quad (16)$$

where $\mathbf{x}_\Gamma$ is the dimensionless position on the biofilm–liquid interface, ϕ^2 is the Thiele number defined as $\phi^2 = (k_{Sm}L_h^2)/(D_S c_{S0})$, the Schmidt number is $\mathrm{Sc} = \nu/D_S$, and $K = K_S/c_{S0}$ is a dimensionless Monod constant. Sh averaged over the biofilm surface is

$$\overline{\mathrm{Sh}} = \overline{\mathrm{Sh}}(\mathrm{Re}, \mathrm{Sc}, \phi^2, K, \text{geometric ratios}). \quad (17)$$

There are at least two geometric factors needed to describe the system geometry. The depth of biofilm valleys is quantified by the roughness, σ. The second measure is the distance between biofilm peaks. If we imagine the biofilm surface shape like a sinusoidal wave, this can be seen as the wavelength. Both measures are geometric factors that should be included in a $\overline{\mathrm{Sh}}$–Re correlation. For reasons that become clear in the following, we lumped the geometric ratios into a single measure, the area enlargement α. It becomes evident from Eq. (17) that both the flux of substrate transferred to the biofilm and the rate of substrate conversion in the biofilm are influenced by factors such as (Bishop et al., 1997): the Reynolds number of the bulk fluid, the biomass activity, and the shape of the biofilm surface. We investigated all these factors at: fluid velocity on the top boundary between 0.01 and 13 cm/s (Re = 0.032 to 32), two biofilm biomass activities (corresponding to $\phi^2 = 32$ and 6.4) and area enlargement between 1 and 2.5. These velocities correspond to normal bulk and average velocities found in biofilm reactors (Kissel, 1986).

Effect of Flow Velocity

First, velocity and concentration fields were calculated for a variety of flow regimes over biofilms with different surface shape. As an example, profiles of the x component of velocity against biofilm depth, for the structure no. 11, in a biofilm valley at $x = 420$ μm, are shown in Fig. 2. Nonzero flow velocities are observed at $y < \delta_{f,max}$, which correspond to the profiles suggested in Fig. 6 from Lewandowski et al. (1995). Moreover, negative velocities at the highest Re indicate the presence of vortices.

Computed contour lines of substrate concentration, at different Re, are shown in Fig. 3a–c for the flat biofilm and in Fig. 3d–f for a rough biofilm. As expected, the average thickness of the CBL strongly decreases with an increase of fluid velocity. The decrease is from 130 (at Re = 0.25) to 24 μm (at Re = 32) for the flat and highly active biofilm (Fig. 4c). This corresponds to an increase in Sherwood number of approximately 5.5 times. Consequently, if external substrate mass transfer rate is increased the biomass is getting higher amounts of substrate. Because oxygen penetrates deeper into the biofilm (Figure 3(a–c)), the overall substrate conversion rate is improved. It can be seen from Table III that a variation from 1.5 to 3.9 g O_2 $m^{-2}_{carrier}$ day^{-1} occurs in the flat biofilm case as Re increases from 0.25 to 32.6. Thus, approximately 2.5 times more substrate is converted (per carrier surface area) in the high-velocity regime than in the low-velocity regime.

For the flat biofilms, the average Sh numbers were very

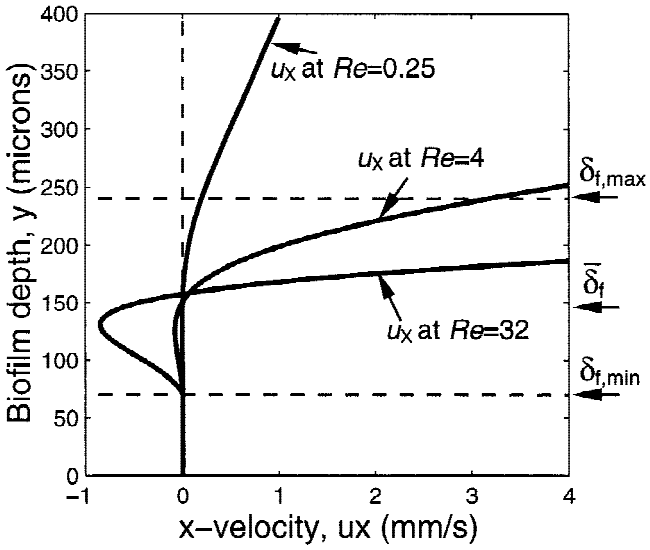

Figure 2. Profiles of the x component of velocity, u_X, against biofilm depth, y, for the structure no. 11, in a biofilm valley at $x = 420$ μm. The maximum biofilm thickness is $\delta_{f,max}$, the minimum biofilm thickness is $\delta_{f,min}$, and the average biofilm thickness is $\bar{\delta}_f = 145$ μm. Velocities in the valley (i.e., at $y < \delta_{f,max}$) are not zero. Moreover, negative velocities at the highest Re indicate the presence of vortices.

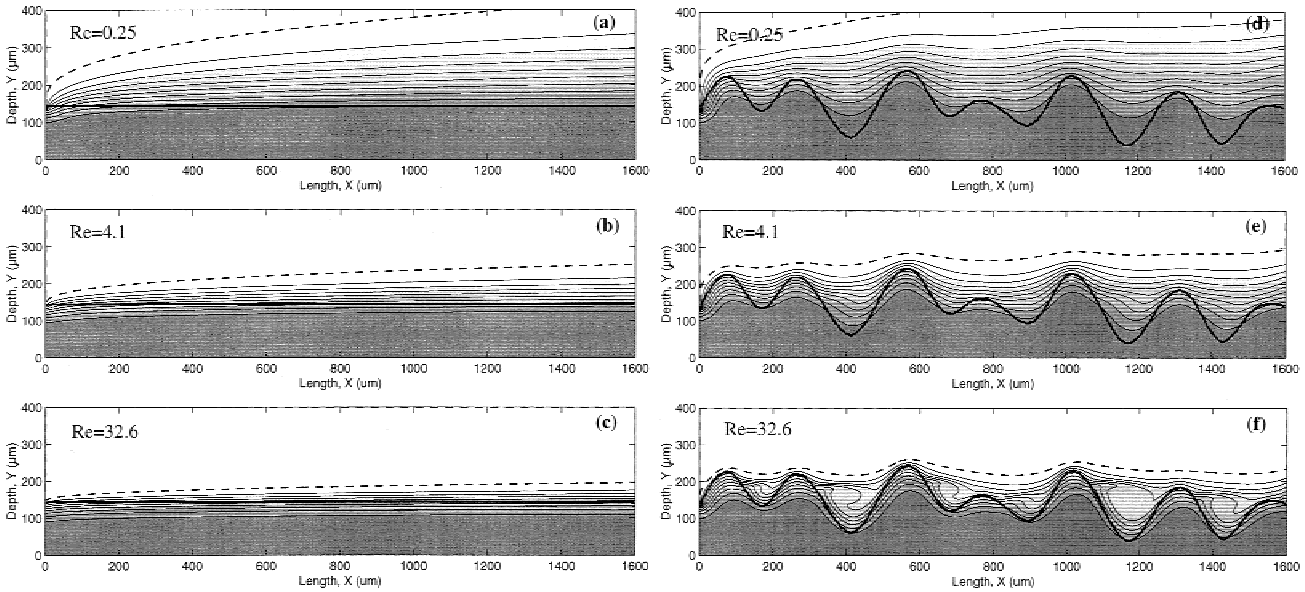

Figure 3. Contour lines of substrate concentration at (a, d) Re = 0.25, (b, e) Re = 4.1, (c, f) Re = 32.6. (a–c) Flat surface biofilm (structure 0); (d–f) rough surface biofilm (structure 11). The biomass is highly active ($k_{Sm} = 1.136 \times 10^{-3}$ kg m^{-3}s^{-1}). Iso-concentration lines show the decrease of substrate concentration from the maximum value in the bulk liquid (white patches) to zero in the biofilm (dark gray patches), with a variation of 10% between lines. Dashed line delimitates the boundary layer at a concentration of 99% from maximum. With a thick line is shown the biofilm–liquid interface.

well correlated with *Re* numbers by functions of the form $\overline{Sh} = C\,Re^{1/3}Sc^{1/3}$. The coefficient C slightly depends on the biofilm activity. We obtained for the cases studied $C = 0.45$ for high-activity biofilm and $C = 0.48$ for low-activity biofilm (Fig. 4a,b). The Sc number was in all cases 434.8. The mass transfer coefficients obtained by this model are in the same range with those measured by Horn and Hempel (1997) at equivalent Re numbers.

For rough biofilms, as those presented in Fig. 3d–f (structure 11 in Table II), mass transfer is also intensified at high liquid velocities. The average CBL thickness decreases from 215 to 50 μm and $\overline{Sh}$ increases only from 1.2 to 5 (see Table III). This means that the external mass transfer is enhanced only 4 times for the structure 11 rough biofilm at an increase of 128 times in flow velocity. The effect of this reduction in mass transfer on global substrate conversion rate in the biofilm is direct. Increase in fluid velocity helped the conversion rate, but not as much as it did for the flat biofilm case.

Effect of Biofilm Surface Shape

As shown in Table III, two aspects resulted from model simulations: (1) mass transfer rates (substrate flux and Sh) and global conversion were always lower in the rough structures studied than in the flat case and (2) the ratio between conversion rates in rough and flat biofilms showed a minimum.

Intuitively, this decrease of mass transport in rough biofilms seems to be contradictory. A very widespread opinion is that roughness has *under any conditions* a favorable effect on mass transfer. Zhang et al. (1994), for example, reported experimental data showing a monotonic enhancement of mass transfer from biofilms with 10 μm to those with 350 μm absolute roughness. The common explanation usually invoked is that overall mass transfer will increase with an increase in biofilm–liquid interfacial area. However, an increase in surface area alone is not enough to increase the global rate of mass transfer.

When the same amount of active biomass has to be distributed over a carrier surface, the biofilm surface can take almost any shape from a very rough to a completely flat one. In the flat case, the CBL follows the biofilm surface closely (dashed line on Fig. 3a–c). However, from Fig. 3d–f it can be seen that for a rough biofilm surface this is not the case. The CBL remains outside the biofilm clusters. Consequently, larger surface area cannot be valued because there is poor convective transport in the voids. This situation is easily visualized in Fig. 3. The mass flux is proportional to the gradient of concentration and its orientation is normal to the iso-concentration lines. It follows that a maximum flux to the biofilm can be reached only when the iso-concentration lines are parallel to the biofilm surface. This can be manifested only if convection is significant between the clusters. Rittmann et al. (1999) also suggested that the flux of substrate per carrier area can be increased in the cluster-and-channel biofilm only if the channels expose more biofilm surface. Presence of only diffusive substrate transport in the valleys creates a disadvantage for the channeled biofilm over the flat one. Microelectrode measurements by de Beer et al. (1995, 1996) showed that at low flow velocities oxygen concentration gradients were perpendicular to the carrier (while the boundary layer was parallel with the carrier), whereas at very high velocities the

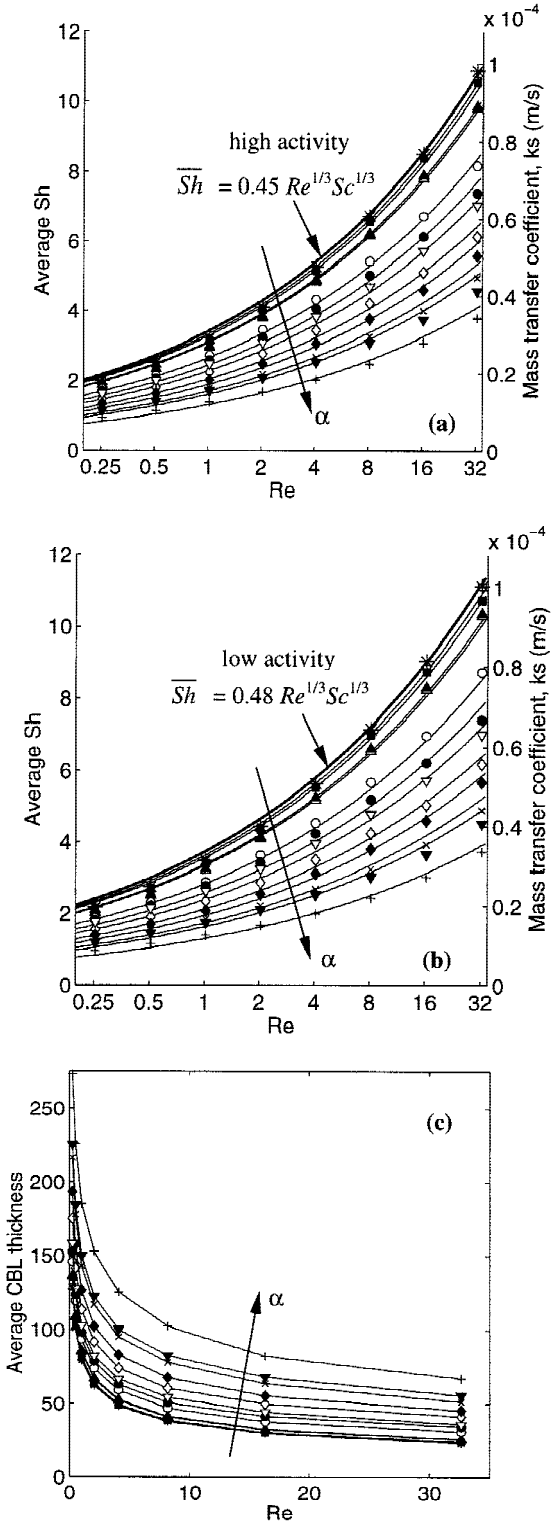

Figure 4. (a, b) Sh numbers and mass transfer coefficients k_s averaged over the carrier length as a function of Re number, at (a) high biofilm activity, and (b) low biofilm activity. Symbols show values of $\overline{Sh}$ and $\overline{k_S}$ obtained for the biofilm shapes in Table II: ✳ (0); □ (1); ■ (2); △ (3); ▲ (4); ○ (5); ● (6); ◇ (7); ◆ (8); ▽ (9); ▼ (10); × (11); + (12). Lines are computed with the correlation $\overline{Sh} = C\alpha^{-n}Re^{1/3}Sc^{1/3}$. (c) Concentration boundary layer thickness at high biofilm activity, calculated from $\overline{k_S}$, as a function of Re number. Symbols like above. Lines are not correlations.

gradients were, more or less, perpendicular to the irregular biofilm surface (while the boundary layer was closely following it). The direct implication would be an increase of mass fluxes relative to the carrier area, as also shown theoretically by Rittmann et al. (1999). However, these experimental studies focused only on isolated biofilm clusters, separated by large areas without biomass. This is obviously the case of a very young biofilm. When surface irregularities develop on a thick base layer, as observed in biofilms grown for many weeks in water treatment systems, our simulations show that even at higher flow velocities over rough biofilms, the concentration boundary layer can still follow the carrier surface. Determining the cases for which heterogeneous biofilms can be modeled as planar structures and the cases for which a multidimensional model is needed, must be the subject of further study.

Examination of the mass transfer coefficient at the biofilm surface clearly shows why the rough structures are not always favorable for mass transport. Due to the waved surface, local k_s, and implicitly its dimensionless form, Sh, are subjected to large variations between the peaks and the valleys of the biofilm structure (Fig. 5). The biofilm peaks are exposed to high gradients of concentration. This generates a high value of Sh or k_s. The flux of substrate in the valleys is by contrast, low. This leads to low values of mass transfer coefficients. On average, the flux enhancement gained in the peak regions can be completely lost in the valleys. As seen in Fig. 5, Sh values for a flat biofilm are on the average indeed larger than those for a rough structure. Fig. 5 also shows that, at low and intermediate Re, Sh approaches its constant, far-downstream value. It can be stated that at least at low Re, the mass entrance length is contained within the length of our system.

Further, we will show by simple numerical calculation why an increased mass transfer area does not necessarily lead to an increased flux of nutrient into the biofilm. Substituting Eq. (7) in (12), followed by integration over the biofilm surface, gives the substrate conversion rate per carrier area, $\Phi_{S,C}$. Hence, $\Phi_{S,C}$ becomes

$$\Phi_{S,C} = \overline{\Phi}_{n,\Gamma} \cdot A_\Gamma / A_C = \overline{\Phi}_{n,\Gamma} \cdot \alpha. \qquad (18)$$

From Eq. (18) we can see that even if the relative biofilm area is enlarged ($\alpha > 1$), a lower value of the average substrate flux normal to the interface can make $\Phi_{S,C}$ decrease. The average substrate flux decreases either due to a higher resistance to mass transfer (lower $\bar{k}_S$) or to a lower driving force $c_{S0} - \overline{c_{S\Gamma}}$. For example, the rough biofilm case presented in Fig. 3e (structure 11, Table II) has twice as much interfacial area as the flat biofilm (structure 0, Fig. 3b), hence $\alpha = 2$. At Re = 4.1, the average Sherwood number is 2.7 for the rough and 5.3 for the flat biofilm (Table III), which translates to average mass transfer coefficients $\bar{k}_s$ of 2.4×10^{-5} and 4.7×10^{-5} m/s, respectively. While $\bar{k}_s$ is halved in the rough biofilm, $\Phi_{S,C}$ decreases by only 13%, from 2.8 g O_2 m^{-2} day^{-1} in the flat structure to 2.47 g O_2 m^{-2} day^{-1} in the rough biofilm. This is because for the rough biofilm the loss of conversion in the valleys is com-

Table III. Average Sh numbers, substrate conversion rate per carrier area and biofilm effectiveness factor for a flat (0) and for a rough (11) biofilm at different Re numbers.[a]

			Flat biofilm (structure 0)			Rough biofilm (structure 11)		
Re	$\overline{Sh}_{11}/\overline{Sh}_0$	$\Phi_{S,C,11}/\Phi_{S,C,0}$	$\overline{Sh}_0$	$\Phi_{S,C,0}$	η	$\overline{Sh}_{11}$	$\Phi_{S,C,11}$	η
0.255	0.59	0.99	1.99	1.51	0.118	1.17	1.50	0.121
0.51	0.57	0.97	2.52	1.79	0.141	1.43	1.74	0.137
1.02	0.55	0.95	3.22	2.09	0.165	1.77	1.98	0.155
2.04	0.53	0.91	4.12	2.44	0.192	2.18	2.22	0.174
4.08	0.51	0.88	5.27	2.81	0.221	2.67	2.47	0.194
8.16	0.48	0.87	6.74	3.17	0.249	3.26	2.77	0.218
16.32	0.47	0.90	8.52	3.46	0.272	4.01	3.13	0.246
32.64	0.45	0.94	10.9	3.86	0.304	4.97	3.64	0.287

[a]The values are calculated for the highly active biofilm.

pensated by a deeper penetration of substrate in the peak areas, and consequently higher conversion there. On the other hand, one could argue that the wavy biofilm structure makes it possible for the biomass clusters to receive a flux of substrate coming from the lateral sides, not only from the top. However, our calculations show that at usual fluid velocities, the main flux of substrate comes from the top and only a small fraction is due to this lateral flux. If only the peaks are accessible for substrate, then at low velocities the "effective" biofilm area is in fact decreased in the rough biofilm case.

An interesting tendency appears at very high flow velocities (i.e., Re > 10, corresponding to bulk velocities greater than 0.2 m/s). From Table III, it can be seen that the disadvantage of the rough biofilm in terms of substrate conversion rate diminishes at high velocities, compared to the flat structure. From Re = 0.4 to Re = 8.2 there was a continuous increase of the flat biofilm advantage in conversion. At Re = 8.2 the flat biofilm converted 15% more substrate than the rough biofilm converted. However, at Re = 32.6 this difference becomes only 6% and a new increasing trend is observed. Although the average mass transfer resistance increases, because of the local improvements of mass transport, the substrate conversion rate increases in the high velocity regimes. Looking at Fig. 3f a qualitative change in the flow pattern can be clearly noticed. Vortices formed in the channels between the clusters, bringing an increased substrate concentration deeper into the biomass. Although vortices begin to form in the cavities also at lower velocities (Fig. 3e), their contribution to mass transfer becomes important only at high bulk velocities. This strongly enhances the local mass transfer coefficients in the valleys. Abnormally high local Sh at Re = 32.6 can be clearly seen in Fig. 5, at x = 350, 650, 850, 1100, and 1400 μm. These conditions are on the back-face of the clusters and on the bottom of valleys, where at low velocities the lowest mass transfer occurs. Note that vortex formation in the cavities does not necessarily mean turbulence. The local flow is still laminar, but this is the beginning of a path to turbulence.

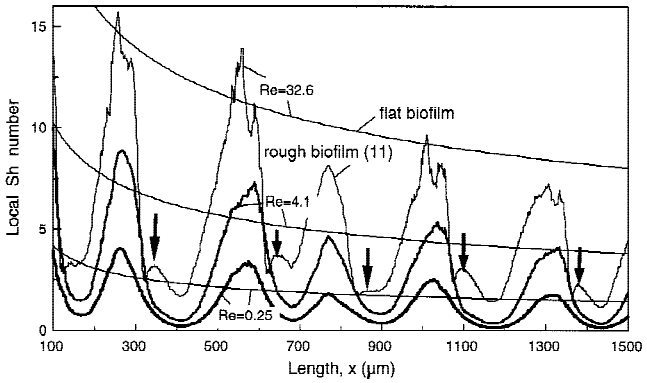

Figure 5. Local Sh number calculated at the biofilm–liquid interface for structure (11) (thick lines), at Re = 0.25, 4.1, and 32.6, are compared with values obtained for the completely flat structure (0) (thin lines). Arrows indicate places where mass transfer enhancement due to vortex formation is clearly visible.

Local significance of convection close to biofilm surface can be proven by comparing local fluxes received at different Re by the biofilm top with those received in the valleys (Fig. 6). As expected, the substrate flux entering the biofilm peak at x = 1300 μm increases linearly with log(Re). In the biofilm valley at x = 1,175 μm, a poor dependence of the flux on Re can be noticed at low bulk velocities. At higher velocities, however, convection due to vortices begins to play an important role in substrate transport. Accordingly, the substrate flux into the biofilm increases dramatically. The relative importance of convection and diffusion in biofilm valleys can be seen by calculating local fluxes in each point of the domain. The local convective and diffusive fluxes are

$$\Phi_C = c_S\sqrt{u_X^2 + u_Y^2} \quad \text{and}$$
$$\Phi_D = D_S\sqrt{(\partial c_S/\partial x)^2 + (\partial c_S/\partial y)^2},$$

respectively. Figure 7 shows in black patches regions where the convective flux was bigger than the diffusive one, and white areas where diffusive flux was dominant. At low Re, diffusion was clearly the main transport mechanism in biofilm valleys. As Re increases, stagnant areas continuously

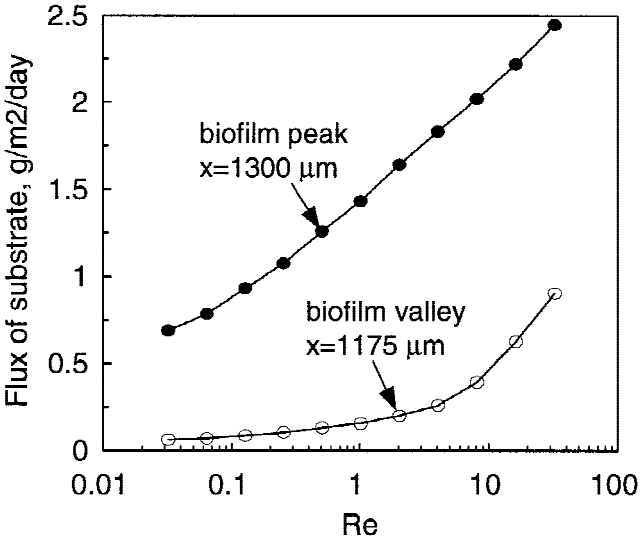

Figure 6. Flux of substrate which enters the biofilm structure 11 (Fig. 3d–f) at $x = 1{,}300$ μm (a biofilm peak) and at $x = 1{,}175$ μm (a biofilm valley) as a function of Re number.

diminish, convection gains importance, and finally dominates diffusive transport.

It appears that an increased convection (and eventually turbulence) will finally lead to an advantage of the rough biofilm over the flat one. Due to stability and accuracy problems with the actual lattice Boltzmann method, it was not possible to simulate the biofilm behavior at Re numbers higher than 64. Refinement of the grid would solve these problems, but higher computational expenses are not justified because the velocities we studied here were already in the range usually reported to occur in biofilm reactors.

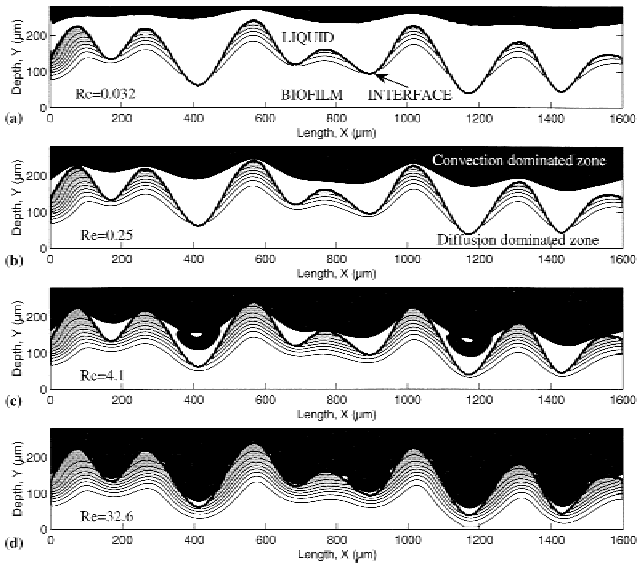

Figure 7. Iso-lines show the decrease of conversion rates (normalized by k_{Sm}) inside a rough biofilm (structure 11) from large values next to the biofilm–liquid interface (gray patches) to zero in the biofilm (white patches), with a variation of 10% between lines. Black areas are zones in the liquid phase where convective flux is bigger than the diffusive flux. The white areas in the liquid show where diffusion dominates.

Effect of Biofilm Activity

Not only geometrical and hydrodynamic factors affect mass transfer and transformation rates in the biofilms. Biofilm activity, the substrate conversion rate constant k_{sm}, obviously influences the global conversion rate and biofilm effectiveness factor. This can be directly seen by comparing the substrate contour lines in Fig. 3e (high activity) with those in Fig. 8e (low activity). While substrate enters only in the superficial layers of the highly active biofilm, the low activity biofilm is completely penetrated. Consequently, the effectiveness factor η is greatly increased in the latter case (see Fig. 10a,b). Despite the fact that biofilm activity was 5 times reduced, the global conversion rate is only 1.5–2 times less in the low-activity case. For external mass transfer coefficients, biofilm activity has much less effect. In general, the low activity biofilms had only slightly better mass transfer coefficients: $\overline{Sh}$ increased 2–9%.

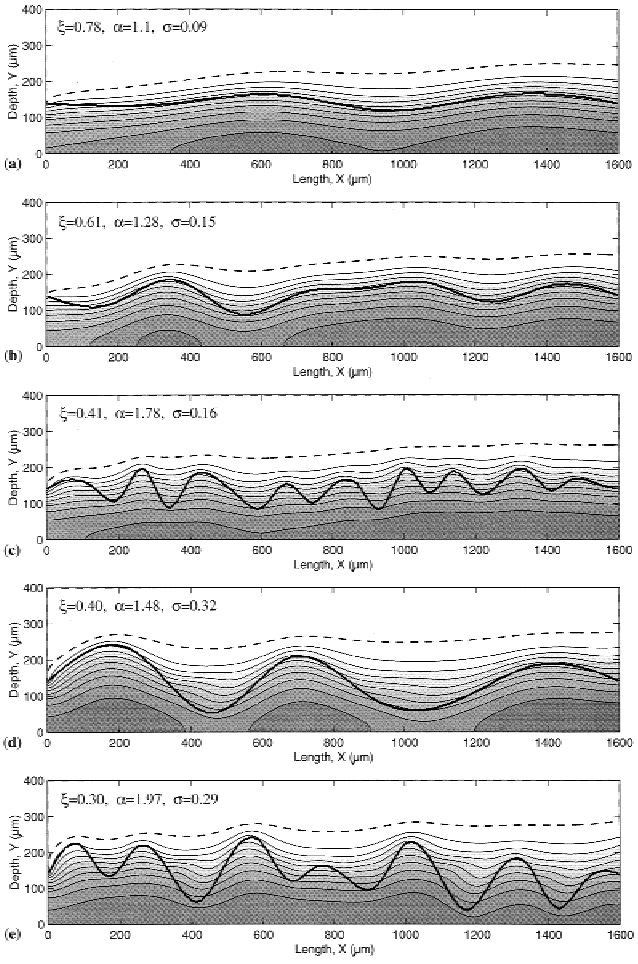

Figure 8. Contour lines of substrate concentration at Re = 4.1 for low activity biofilm. Graphs correspond to structures 3 (a), 5 (b), 8 (c), 9 (d), and 11 (e) from Table II. Iso-concentration lines show the decrease of substrate concentration from the maximum value in the bulk liquid (white patches) to zero in the biofilm (dark gray patches), with a variation of 10% between lines. Dashed line deliminates the boundary layer at a concentration of 99% from maximum. With a thick line is shown the biofilm–liquid interface.

Correlations Between Biofilm Structure, Mass Transfer, and Conversion

Investigating only qualitatively the relevant factors that might influence mass transfer and transformation in rough biofilms is not enough. The ultimate goal is to find correlations between biofilm structural parameters and transport and conversion measures. If possible, these correlations should be presented as equations including dimensionless numbers. If appropriately applied, these equations can be very useful in the design and operation of biofilm reactors. One could answer in a quantitative way questions like: in what type of biofilm will be mass transfer enhanced and under what conditions? or, is substrate conversion increased by this biofilm structure? or, is this bioreactor suitable to grow a certain type of biofilm?

The first step must be identification of the relevant parameters. To do this, we focused our attention on three possible biofilm structural measures: roughness (σ), area enlargement (α) and compactness (ξ) (see Fig. 8). Diagrams of conversion rate per carrier area against σ, α, and ξ were made for all Re numbers. The same was done for the average Sh numbers of different structures. Such examples at Re = 4.1 are shown in Fig. 9. It is usually believed (Zhang et al., 1994; Bishop et al., 1997) that the absolute roughness is the geometrical measure the most responsible for the observed differences in mass transfer between diverse biofilms. However, roughness is only a measure of the depth of biofilm valleys. Although there is a decreasing tendency of conversion rate and $\overline{Sh}$ at increased roughnesses, the correlation is not very good. Good examples to explain these deviations are structures 5 and 8. These cases have very similar roughness coefficients, but the computed conversion rates and especially $\overline{Sh}$ numbers differ strongly (see Fig. 9). Referring to Fig. 8b,c, although both cases are for a biofilm roughness of about 50 μm, structure 8 has a higher frequency of the cluster-channel pattern. In other words, not only the depth of the channels but also their width influences the mass transfer. The wider the valleys the higher the mass transfer rate. Narrow channels cannot establish significant convective mass transfer and thus they are less favorable. The same effect can be seen also on structures 9 (Fig. 8d) and 11 (Fig. 8e). Both have an absolute roughness of about 100 μm, but while structure 9 has valleys 600 μm apart, structure 11 has gaps only 300 μm apart, and consequently a lower mass transfer rate.

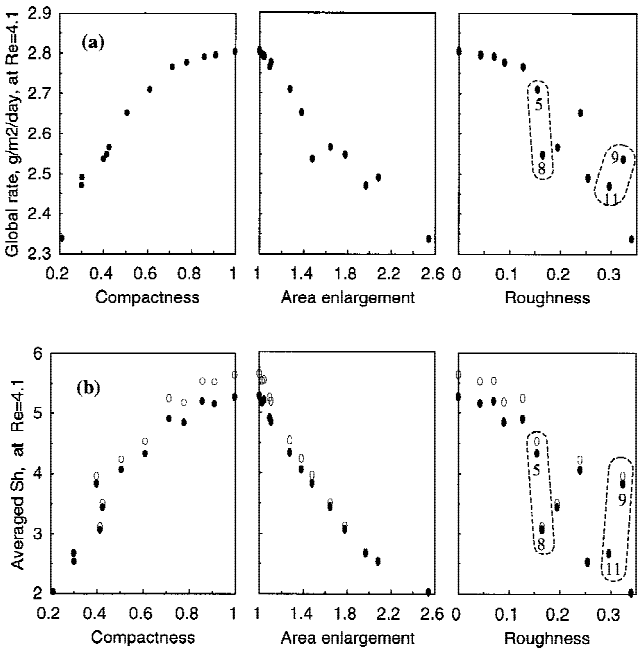

Figure 9. (a) Global oxygen conversion rate in the biofilm related to the carrier surface area ($\Phi_{S,C}$) as a function of biofilm compactness, area enlargement and roughness at high biofilm activity and Re = 4.1. Numbers indicate structures discussed in text. (b) Sherwood number averaged over the biofilm surface as a function of biofilm compactness, area enlargement and roughness at Re = 4.1 for high (●) and low (○) biofilm activity.

Conversion rate and $\overline{Sh}$ correlated well with surface compactness and area enlargement (see Fig. 9). Conversion shows a slight decrease when compactness decreases from its maximum (the flat biofilm case) to about 0.7 and then it drops substantially for very channeled biofilms. An almost linear decrease of both conversion and mass transfer coefficients can be seen with an enlargement of the biofilm per carrier area ratio. It seems from Fig. 9 that the global substrate conversion rate correlates better to the compactness, whereas the average Sherwood number correlates well with the biofilm area enlargement. This seems reasonable knowing that both compactness and conversion rate quantify volumetric properties, while area enlargement and mass transfer coefficient are measures related to surfaces.

Recognizing the usefulness of compactness, diagrams showing the conversion rate and biofilm effectiveness factor for different biofilm structures, at different flow velocities were constructed (Fig. 10). At low Re, the conversion rate is not significantly influenced by compactness but differences up to 20% occur at high Re regimes. It can be noticed again, that at the highest velocities, structures with wide channels reach higher conversions than do those with dense and narrow channels (compare structure 8 with 9, or 10 with 11). This effect can be attributed to an easier vortex formation in biofilms with large valleys. Anyway, relative to the flat case, conversion in all very rough biofilms increases at very high Re. At lower biofilm activity, the effects of surface structure are less pronounced (note the expanded scale for low activity).

By examining Fig. 10 we note that, at high liquid velocities, the conversion rate can be slightly greater than for the completely flat biofilm case. This happens only when the biofilm surface has a small roughness. Only in this case (see Fig. 8a), the concentration boundary layer can follow the biofilm surface, without vortex development.

Given a very clear dependency on area enlargement can be observed for the external mass transfer parameters like Sh or k_s (Fig. 9b), we chose to include this structural parameter in the $\overline{Sh}$–Re correlation. The proposed empirical correlation is a product of power functions:

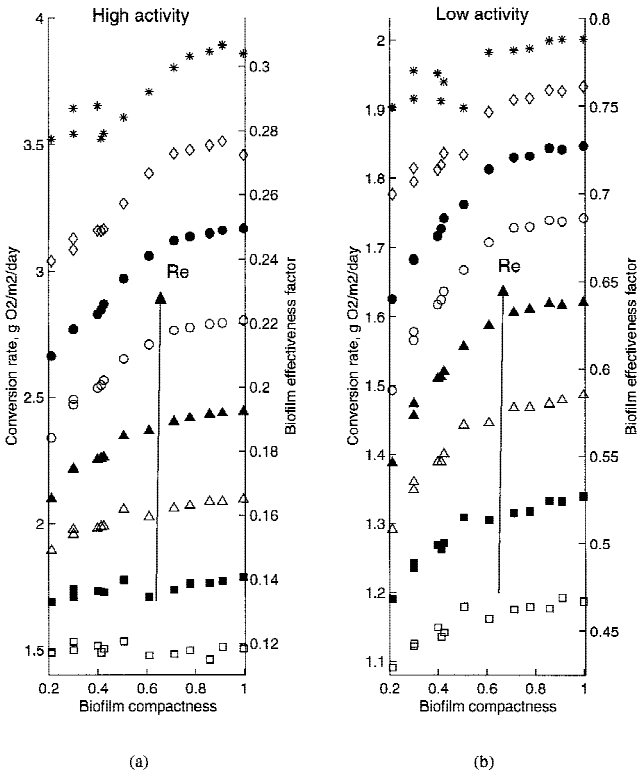

Figure 10. Global oxygen conversion rate in the biofilm related to the carrier surface area ($\Phi_{S,C}$) and global biofilm effectiveness factor (η) as a function of biofilm compactness (ξ), at (a) high biofilm activity (b) low biofilm activity. Symbols represent simulation results at different Re numbers: □ 0.25; ■ 0.51; △ 1.02; ▲ 2.04; ○ 4.08; ● 8.16; ◇ 16.32; ✳ 32.6.

$$\overline{\mathrm{Sh}} = \frac{C}{\alpha^n}\,\mathrm{Re}^{1/3}\mathrm{Sc}^{1/3}. \tag{19}$$

All $\overline{\mathrm{Sh}}$–Re data obtained were correlated with this function. Results are presented in Fig. 4a (highly active biofilm) and Fig. 4b (less active biofilm). For the high-activity biofilm, the coefficients were $C = 0.45$ and $n = 1.034$. In the low-activity biofilm, we obtained $C = 0.478$ and $n = 1.12$. The correlation is good for low Re but becomes worse at high Re. The maximum error was 10% at Re = 32.6 for structure 7.

The correlation should not be interpreted as a result valid for mass boundary layer entrance on flat plate. The boundary layer theory predicts in that case that Sh increases with Re at power ½. Due to the Couette-like driven flow in this system and the periodic boundaries in the flow direction, Sh is a function of $\mathrm{Re}^{1/3}$. This correlation should rather be seen as a theoretical example on how biofilm shape characteristics can be included in mass transfer/momentum transfer dependency.

Validity of the Model for Practical Biofilms

A major problem could question the validity of results found using this model because 2-D flow is obviously different from 3-D flow. If instead of a ridge-like structure the biofilms presented a "dome" morphology, then the flow could find a preferential path around the biofilm towers, and not over them. Mass transfer could be increased, especially if the ridges extend along the main flow direction and not across it, like in the 2-D case. Results from the present 2-D model can be applied directly only for ridges-like biofilms, as obtained by Gjaltema et al. (1994) in a rotating annular reactor. A 3-D model for convection-diffusion-reaction in rough biofilms is now under development (Eberl et al., 1999). Preliminary results of this three-dimensional model show however that no important qualitative differences appear. The same tendency of mass transport and conversion rates to decrease when the biofilm area enlargement increases was predicted, and values very close to the 2-D simulations were obtained. Complete results will be published in a forthcoming article.

The present model considers the biofilm volume as a rigid object. Many biofilms are in reality gelatinous, flexible structures. Biofilm oscillations induced by the flow can therefore occur (Stoodley et al., 1998). They create turbulence and obviously increase mass transfer. This might be a cause of enhanced mass transfer rates in rough biofilms reported in the literature (Siegrist and Gujer, 1985; Zhang et al., 1994). Situations as those predicted by the model at the highest velocities are less likely to occur in reality. First, because biofilms grown at high velocities (and implicitly high shear rates) usually appear to be smooth (Kugaprasatham et al., 1992). Breaking and sloughing due to biofilm vibrations and high shear forces will frequently occur. And second, vortex formation is impeded in a three-dimensional biofilm compared to 2-D biofilm having the same area enlargement, because the fluid can easier find ways to bypass the clusters.

The comparison between conversion rates achieved in structures with different geometries, can be done in the most reasonable way by distributing the biomass uniformly in the whole biofilm. Another realistic assumption would be to have highly active biomass in the top layers, and less active in the biofilm depth. We believe that this assumption will enhance even more the performance of the flat biofilm compared to the rough one. If biomass decays in the valleys, "waiting for food that never arrives," then the effective reaction volume in rough biofilms decreases (compared to uniform distribution), being restricted only to the peak areas. Consequently, the global substrate uptake rate will decrease. Moreover, this biomass segregation will generate even more roughness because peaks would grow faster, deepening the channels. However, a realistic non-uniform biomass distribution can be realized only in a model including biomass growth and decay, which is the scope of a further publication.

A preliminary study on the importance of biofilm voids on convective nutrients transport in biofilms has also been made. Two protuberances from the structure 11 were pierced with tunnels. The diameter of those pores was chosen to be about 30 μm, a value reported as typical in Stoodley et al. (1994) and de Beer et al. (1994). Two simulations

were carried out. In the first case, fluid was allowed to flow through the pores (Fig. 11a). In the second one the pores were closed for flow, but they were kept empty of biomass (Fig. 11b). This was done to ensure that the same total amount of biomass exists in both systems, whether the pores were open or clogged. Model results show that only at very high liquid velocity in the bulk, flow through the pores brings an important contribution to substrate transport in the biofilm (Fig. 11a,b). Only above a critical Re number do the benefits of convective substrate transport through pores become important. Great care must be taken in interpreting these results. Not only the pores diameter is important but also their length, position and orientation with respect to the main flow direction. Longer pores necessitate a larger pressure difference to promote the flow. Pores at the biofilm bottom are positioned usually in regions with stagnant or very slowly moving liquid. Consequently, their contribution to mass transport will be negligible. It must be also noticed that in our 2-D simulations pores do not have a cylindrical shape. In a real 3-D space, friction through cylindrical pores would be much increased relative to these planar pores. Thus, in all situations presented above, convective substrate transport will be even more decreased, both due to insufficient driving force and to increased frictional resistance. The complete three-dimensional model needed to quantitatively evaluate substrate transport through biofilm pores will be presented elsewhere (Eberl et al., in preparation).

If only diffusion is important in pores and valleys, rough biofilms behave as if they were compact but having less biomass activity. Therefore, in the absence of convection in the valleys (i.e., low Re regime), one-dimensional diffusion-reaction models could be adequate to predict overall substrate conversion rates. A first comparison between one- and multidimensional biofilm models was made in Morgenroth et al. (1999).

CONCLUSIONS

A two-dimensional model was used to compute laminar fluid flow and substrate mass transport in irregularly shaped biofilms. By using this model, it was possible to make a theoretical prediction of the influence of biofilm geometrical characteristics on global substrate mass transfer and conversion rates. Although computations are performed in the laminar hydrodynamic boundary (sub)layer, flow in the bulk liquid can be either in the laminar or in the turbulent regime.

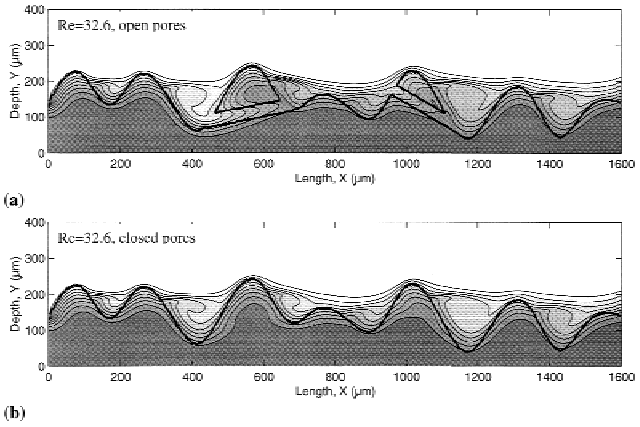

Figure 11. Substrate concentration contour plots in the case with (a) open pores and (b) closed pores. All simulation parameters were similar to those of the case shown in Fig. 3d–f.

The main result of this study is that increased biofilm roughness does not necessarily lead to an enhancement of either conversion rates or external mass transfer. If there is poor convection in the biofilm channels or valleys, then the main transport mechanism for substrate is only by diffusion, driven by gradients of concentration perpendicular to the carrier. The overall mass transfer rate decreases in rough biofilms because of an increase in the diffusional path of substrate. Although the total biofilm area is increased by roughness, the effective mass transfer area is in fact decreased. Only a very limited fraction of all biofilm area receives nutrient because only the peaks are accessible for substrate.

External mass transfer rates were greatly increased at higher flow velocities. A variation of Re number over 2 orders of magnitude produced mass transfer coefficients five times larger. However, the global substrate conversion rates per carrier area were less affected. Only approximately 2.5 times larger rates at the highest flow velocity than at the lowest were predicted. The results of this study clearly indicate that interpretation of local concentration or flow measurements as such might easily lead to erroneous interpretation of biofilm conversion processes. Only evaluation of overall conversion rates of mass fluxes can describe the correct biofilm conversion.

The influence of flow, biofilm geometry and activity on external mass transfer can be quantified by $\overline{Sh}$–Re correlations. The average Sh in our model system varied proportionally with $Re^{1/3}$. Area enlargement gave the best correlation with mass transfer parameters. In the velocity range investigated, Sh was inversely proportional to area enlargement at a power close to 1. The biofilm activity had only a small effect on mass transfer coefficients.

Conversion rates were well correlated by biofilm compactness. The more compact the biofilm the higher the global conversion rate of substrate. Our study demonstrates that roughness alone is not enough to characterize the influence of surface irregularity on mass transport and conversion. If biofilm peaks are not far enough from each other, convective transport in valleys cannot significantly contribute to the increase of the total conversion rate. A study of mass transfer in biofilms with more complicated surface shape should therefore not lump roughness and cluster frequency into a single measure, but rather consider them separately.

At low flow velocity, the effect of biofilm roughness on the total conversion rate per carrier area was almost negligible. This can be explained by the fact that in the low velocity regime the surface irregularities are deep inside the CBL. Because the concentration boundary layer is very thick, the overall biofilm effectiveness is determined by the

external mass transfer rate. If only diffusion occurs in pores and valleys, rough biofilms behave as if they were compact but having less biomass activity. At higher flow velocities, the importance of convective transport increases. Nevertheless, even in convective transport dominated regimes the overall conversion can be decreased due to an irregular biofilm surface.

This research was sponsored by the Netherlands Organisation for Applied Scientific Research (TNO) by the contract 95/638/MEP. The authors acknowledge Hermann Eberl for many critical and conceptual suggestions.

References

Bishop PL, Gibbs JT, Cunningham BE. 1997. Relationship between concentration and hydrodynamic boundary layers over biofilms. Environ Technol 18:375–386.

Chen S, Doolen GD. 1998. Lattice Boltzmann method for fluid flows. Annu Rev Fluid Mech 30:329–364.

De Beer D, Stoodley P, Roe F, Lewandowski Z. 1994. Effects of biofilm structures on oxygen distribution and mass transport. Biotechnol Bioeng 43:1131–1138.

De Beer D, Stoodley P. 1995. Relation between the structure of an aerobic biofilm and transport phenomena. Water Sci Technol 32(8):11–18.

De Beer D, Stoodley P, Lewandowski Z. 1996. Liquid flow and mass transport in heterogeneous biofilms. Water Res 30(11):2761–2765.

Deen WM. 1998. Analysis of transport phenomena. New York: Oxford University Press.

Eberl H, Picioreanu C, van Loosdrecht MCM. 1999. Modelling geometrical heterogeneity in biofilms. In: Proceedings of The 13th International Conference of High Performance Computing Systems & Applications, June 1999, Kingston, Canada.

Fogler HS. 1992. Elements of Chemical reaction engineering. 2nd edition. Englewood Cliffs, NJ: Prentice-Hall, Inc.

Gjaltema A, Arts PAM, van Loosdrecht MCM, Kuenen JG, Heijnen JJ. 1994. Heterogeneity of biofilms in rotating annular reactor: Occurrence, structure and consequences. Biotechnol Bioeng 44:194–204.

Horn H, Hempel DC. 1995. Mass transfer coefficients for an autotrophic and a heterotrophic biofilm system. Water Sci Technol 32(8):199–204.

Horn H, Hempel DC. 1997. Substrate utilization and mass transfer in an autotrophic biofilm system: Experimental results and numerical simulation. Biotechnol Bioeng 53:363–371.

Kissel JC. 1986. Modeling mass transfer in biological wastewater treatment processes. Water Sci Technol 18(6):35–45.

Kugaprasatham S, Nagaoka H, Ohgaki S. 1992. Effect of turbulence on nitrifying biofilms at non-limiting substrate conditions. Water Res 26(12):1629–1638.

Lewandowski Z, Stoodley P, Altobelli S. 1995. Experimental and conceptual studies on mass transport in biofilms. Water Sci Technol 31(1): 153–162.

Morgenroth E, Eberl H, van Loosdrecht MCM. 1999. Evaluating 3-D and 1-D mathematical models for mass transport in heterogeneous biofilms. In: Proceedings of the 4th IAWQ Conference on Biofilm Systems, New York, October 17–20, 1999.

Murga R, Stewart PS, Daly D. 1995. Quantitative analysis of biofilm thickness variability. Biotechnol Bioeng 45:503–510.

Picioreanu C, van Loosdrecht MCM, Heijnen JJ. 1998. Mathematical modeling of biofilm structure with a hybrid differential-discrete cellular automaton approach. Biotechnol Bioeng 58(1):101–116.

Picioreanu C, van Loosdrecht MCM, Heijnen JJ. 1999. Discrete-differential modelling of biofilm structure. Water Sci Technol 39(7): 115–122.

Picioreanu C. 1999. Multidimensional modeling of biofilm structure. Ph.D. thesis, Delft University of Technology, Delft (ISBN 90-9013310-0).

Ponce Dawson S, Chen S, Doolen GD. 1993. Lattice Boltzmann computations for reaction–diffusion equations. J Chem Phys 98(2): 1514–1523.

Rittmann BE, Pettis M, Reeves HW, Stahl DA. 1999. How biofilm clusters affect substrate flux and ecological selection. Water Sci Technol 39(7): 99–105.

Siegrist H, Gujer W. 1985. Mass transfer mechanisms in a heterotrophic biofilm. Water Res 19(11):1369–1378.

Stoodley P, de Beer D, Lewandowski Z. 1994. Liquid flow in biofilm systems. Appl Environ Microbiol 60(8):2711–2716.

Stoodley P, Yang S, Lappin-Scott H, Lewandowski Z. 1997. Relationship between mass transfer coefficient and liquid flow velocity in heterogeneous biofilms using microelectrodes and confocal microscopy. Biotechnol Bioeng 56:681–688.

Stoodley P, Lewandowski Z, Boyle JD, Lappin-Scott HM. 1998. Oscillation characteristics of biofilm streamers in turbulent flowing water as related to drag and pressure drop. Biotechnol Bioeng 57(5):536–544.

Stoodley P, Boyle JD, de Beer D, Lappin-Scott HM. 1999. Evolving perspectives of biofilm structure. Biofouling 14(1):75–90.

Tijhuis L, van Loosdrecht MCM, Heijnen JJ. 1994. Formation and growth of heterotrophic aerobic biofilms on small suspended particles in airlift reactors. Biotechnol Bioeng 44:595–608.

Van Benthum WAJ, van Loosdrecht MCM, Tijhuis L, Heijnen JJ. 1995. Solids retention time in heterotrophic and nitrifying biofilms in a biofilm airlift suspension reactor. Water Sci Technol 32(8):53–60.

Wanner O, Reichert P. 1996. Mathematical modeling of mixed-culture biofilms. Biotechnol Bioeng 49:172–184.

Zhang TC, Bishop PL, Gibbs JT. 1994. Effect of roughness and thickness of biofilms on external mass transfer resistance. In: Critical Issues in Water and Wastewater Treatment, National Conference in Environmental Engineering. New York: ASCE. p 593–600.